Sustainable Carbon Materials

https://doi.org/10.48130/scm-0026-0018

Original Research

Open Access

An atom-level insight into the oxide support effect of Ni-based catalysts on the syngas production in methane reforming

Yuangu Xia[1], Haoyu Wang[1], Bin Hu[1], Huaide Sun[1], Tahir Iqbal[2], Ji Liu[1*] and Qiang Lu[1*]

Received: 8 January 2026

Revised: 2 March 2026

Accepted: 7 April 2026

Published online: 11 May 2026

Abstract

The rational design of highly efficient and stable catalysts is pivotal for the sustainable carbon source-derived methane reforming. The support material governs both the catalytic activity and long-term stability directly, by providing the surface acid/base sites and regulating strong metal-support interaction (SMSI). However, a comprehensive atomic-level understanding of how different oxide supports influence catalytic performance remains lacking. In the present study, a series of catalyst models that consist of common oxide supports and a Ni_4 cluster were employed to elucidate support effects, using bulk Ni(111) as a reference. The catalytic properties, such as reactivity and carbon deposition tendency, were evaluated by mainly examining the adsorption of reactants (CH_4, CO_2, H_2O), key intermediates (CH, C, O, H, OH), and products (CO, H_2) on Ni_4/MO_n models. Notably, the Ni_4 cluster supported on Al_2O_3(110), ZrO_2(111), and MgO(100) generally enhances the reaction by strengthening the adsorption of reactants and cracking intermediates. However, excessively strong adsorption of carbon-containing intermediates on MgO also increases the risks of carbon deposition and CO poisoning. ZrO_2 emerges as a more balanced support, providing moderate activity enhancement while inherently suppressing carbon deposition. In contrast, Ni_4 clusters are redispersed into single atoms on SiO_2(110), resulting in significantly weaker reactivity. This work elucidates the tailoring effect of supports on adsorption properties and activity-stability trade-off, offering a theoretical basis for the rational design of methane reforming catalysts.

Keywords: Methane reforming, Support influence, Adsorption, DFT

Highlights

- Reactivity of supported Ni-based catalysts is significantly different from that of bulk Ni(111).
- MgO, Al_2O_3, ZrO_2 enhance the activity of Ni clusters by promoting reactant/intermediate adsorption.
- ZrO_2 offers an appropriate balance between the Ni cluster reactivity and carbon deposition.

* Correspondence: Ji Liu (liujipower@126.com); Qiang Lu (qianglu@mail.ustc.edu.cn or qlu@ncepu.edu.cn)

Full list of author information is available at the end of the article.

https://doi.org/10.48130/scm-0026-0018

Graphical abstract

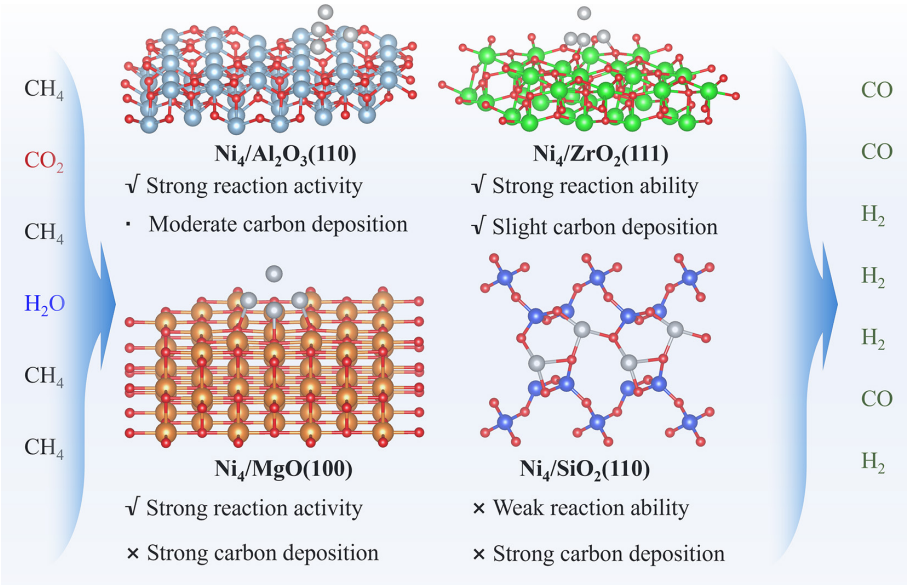

Introduction

Biomass stands as a pivotal sustainable carbon source that offers a renewable pathway to platform chemicals such as methane via gasification[1]. The reforming of biomass-derived methane presents an efficient route to produce green syngas (CO + H_2), a fundamental feedstock for industrial chemical synthesis. Catalytic conversion by adopting Ni-based catalysts is the main route for methane reforming, and the support is essential for the optimized activity and stability[2]. Concurrently, it is widely recognized that electronic structure modification by different supports plays a decisive role in determining catalytic activity and stability[3–5], for instance, via the surface acidity/basicity[6] and strong metal-support interaction (SMSI)[7]. They can refine the adsorption of reactants and intermediates, while SMSI can also inhibit metal particle agglomeration to enhance catalyst stability[8,9].

The predominant supports for Ni-based catalysts are oxide substrates, encompassing Al_2O_3, ZrO_2, MgO, and SiO_2[10–13]. Among these, Al_2O_3 exhibits exceptional mechanical strength, and the intrinsic pore architecture facilitates effective dispersion of Ni particles[14,15], while surface acidic sites promote methane adsorption and activation through enhanced C–H bond cleavage. Nevertheless, the phase transition can induce sintering of active sites, compromising catalytic performance. ZrO_2 demonstrates remarkable crystal phase stability at elevated temperatures (> 800 °C), effectively suppressing Ni particle aggregation while simultaneously inhibiting carbon deposition[16,17]. The basic sites of MgO enhance chemical adsorption and activation of CO_2 during methane dry reforming. Furthermore, SMSI facilitates electron transfer from the support to the active components, thereby activating the active species and reducing the energy barrier for methane reforming[18–20]. SiO_2 presents a well-developed pore structure coupled with relatively low chemical reactivity, primarily providing a chemical environment conducive to Ni component dispersion. Notably, mesoporous zeolites can encapsulate active Ni species, making them ideal supports suitable for harsh operating conditions. However, their inherent weak metal-support interactions may also compromise active site stability[21,22].

Given that different supports can fundamentally alter catalytic activity, a comprehensive understanding of how various supports influence methane reforming is imperative. This study focuses on four common support surfaces—Al_2O_3(110), ZrO_2(111), MgO(100), and SiO_2(110)—that have been extensively observed in experiments. Employing density functional theory (DFT) calculations, we systematically investigated the influence of supports on the active Ni component and the adsorption behaviors of key reaction intermediates. The investigation provides microscopic insights into SMSI phenomena and establishes a theoretical foundation for the rational design of high-performance methane reforming catalysts.

Computational details

The optimized lattice parameters for the investigated materials are as follows: α-Al_2O_3 exhibits hexagonal symmetry with a = b = 4.81 Å and c = 13.12 Å; monoclinic ZrO_2 (m-ZrO_2) displays lattice constants of a = 5.15 Å, b = 5.23 Å, c = 5.33 Å, and β = 99.2°; face-centered cubic MgO presents a lattice parameter of a = b = c = 4.19 Å; and trigonal SiO_2 shows lattice parameters of a = b = 4.91 Å, c = 5.43 Å, and γ = 120°. Based on experimental observations demonstrating their stability under methane reforming conditions[23,24], the Al_2O_3(110), *m*-ZrO_2(111), MgO(100), and SiO_2(110) surfaces were selected for theoretical model construction. A Ni_4 cluster was employed as the active catalytic component, positioned on the respective support surfaces.

Spin-polarized DFT calculations were performed using the Vienna ab initio simulation package (VASP)[25]. The Perdew-Burke-Ernzerhof (PBE) exchange-correlation functional was employed in conjunction with projected-augmented wave (PAW) pseudopotentials, utilizing a plane-wave cutoff energy of 400 eV. The *k*-point mesh resolution value was set to 0.03 (2π/Å) for all calculations. The convergence accuracies of electron self-consistent field and force during geometry optimization were 1×10^{-6} eV and −0.04 eV/Å, respectively. The Grimme D3 correction was considered in all calculations[26]. A vacuum layer of 15 Å was implemented to eliminate spurious interactions between periodic images. Structural visualization and computational output analysis were conducted using VESTA[27] and

VASPKIT[28] packages, respectively. The adsorption energy was determined according to Eq. (1).

$$E_{ads} = E_{total} - E_{slab} - E_{gas} \quad (1)$$

where, the E_{ads}, E_{total}, E_{slab}, and E_{gas} are the adsorption energy, the total energy of the adsorbed slab system, the energy of the pristine slab, and the energy of the isolated gaseous molecule.

The electron density difference (EDD, $\Delta\rho$) is calculated as follows:

$$\Delta\rho = \rho_{a+b} - \rho_a - \rho_b \quad (2)$$

where, the ρ_{a+b}, ρ_a, and ρ_b are the electron density distributions of complex a and b, single a, and single b. Furthermore, density of states (DOS) and crystal orbital Hamilton population (COHP) analyses were utilized to elucidate the electronic interactions between adsorbate species and adsorbent surfaces.

Results and discussion

The composite structure of Ni_4/MO_n (M=Al, Zr, Mg, Si)

The optimized structures and EDD diagrams for the Ni_4 cluster supported on Al_2O_3(110), ZrO_2(111), MgO(100), and SiO_2(110) are shown in Fig. 1, together with the corresponding binding energies between the active clusters and their respective substrates.

On the Al_2O_3(110) surface, the Ni_4 cluster adopts a tetrahedral configuration, wherein two Ni atoms coordinate with surface Al atoms and a third Ni atom binds to surface O atoms. EDD analysis reveals electron accumulation in the interfacial region, originating from both the Ni_4 cluster and adjacent surface atoms, which signifies a robust metal-support interaction corroborated by a substantial binding energy of −6.13 eV. Similar interaction patterns are observed for Ni_4 clusters on ZrO_2(111) and MgO(100) surfaces, exhibiting binding energies of −5.29 and −2.85 eV, respectively, with slight electron transfer between the Ni_4 cluster and the substrate. Bader charge analysis reveals distinct electron transfer behaviors between the Ni_4 cluster and oxide substrates. The calculated Bader charges of the Ni_4 fragment are −1.201 |e|, +0.078 |e|, and −0.368 |e| for the Ni_4/Al_2O_3(110), Ni_4/ZrO_2(111), and Ni_4/MgO(100) systems, respectively. These small charge perturbations indicate that the Ni_4 cluster retains its intrinsic metallic character across all three supports, with the main charge redistribution at the cluster-substrate interface. In contrast, the Ni_4/SiO_2(110) system displays a fundamentally different interaction mechanism: the four Ni atoms become individually dispersed and embedded within the support surface, with each Ni atom coordinating to three O atoms. This configuration yields an exceptionally high binding energy of −22.78 eV. Consistently, EDD analysis reveals substantial charge redistribution across the entire surface. The pronounced positive charge accumulation on the Ni_4 cluster (+4.021 |e|) indicates a markedly ionic character, arising from the individual coordination of all Ni atoms with surface O and Si sites. This substantial electron depletion elucidates the exceptionally strong interfacial binding between Ni_4 and the SiO_2(110) surface.

The adsorption of methane reforming-related species on Ni_4/MO_n

Guided by the mechanistic framework of methane steam and dry reforming reactions, we systematically investigated the adsorption behaviors of key surface species, including CH_4, CO_2, H_2O, CO, H_2, CH, C, O, OH, and H across various catalyst surfaces. Multiple adsorption sites were comprehensively examined, as illustrated in Fig. 1. For the Ni_4/Al_2O_3(110), Ni_4/ZrO_2(111), and Ni_4/MgO(100) systems, distinct Ni_4 cluster sites, interfacial sites, and support sites were identified and evaluated. In the case of Ni_4/SiO_2(110), a unique set of adsorption sites was specifically characterized, encompassing single Ni, Si, and O sites, as well as their bridge sites. The adsorption energies of all investigated species on these catalyst surfaces, as well as on the reference Ni(111) surface, are compiled in Supplementary Tables S1–S5 and Supplementary Figs S1–S4. Meanwhile, Fig. 2 and Supplementary Table S6 summarizes the highest adsorption energy of all reaction species on various catalysts, with detailed analysis in the subsequent sections.

The adsorption of reactants (CH_4, CO_2, and H_2O)

The adsorption of the reactant CH_4 constitutes a critical initial step in the reforming process, and CO_2 and H_2O serve as the fundamental feedstocks for methane dry and steam reforming. All reactants exhibit distinct adsorption behaviors across various supported catalysts.

CH_4 preferentially adsorbs atop the Ni_4 cluster on Ni_4/Al_2O_3(110) (Fig. 3), with an E_{ads} of −0.34 eV. EDD analysis reveals electron depletion from the H atoms of CH_4 toward the interfacial region between the Ni cluster and C atom, corroborated by DOS mapping, which demonstrates significant orbital overlap between the C 2p orbitals

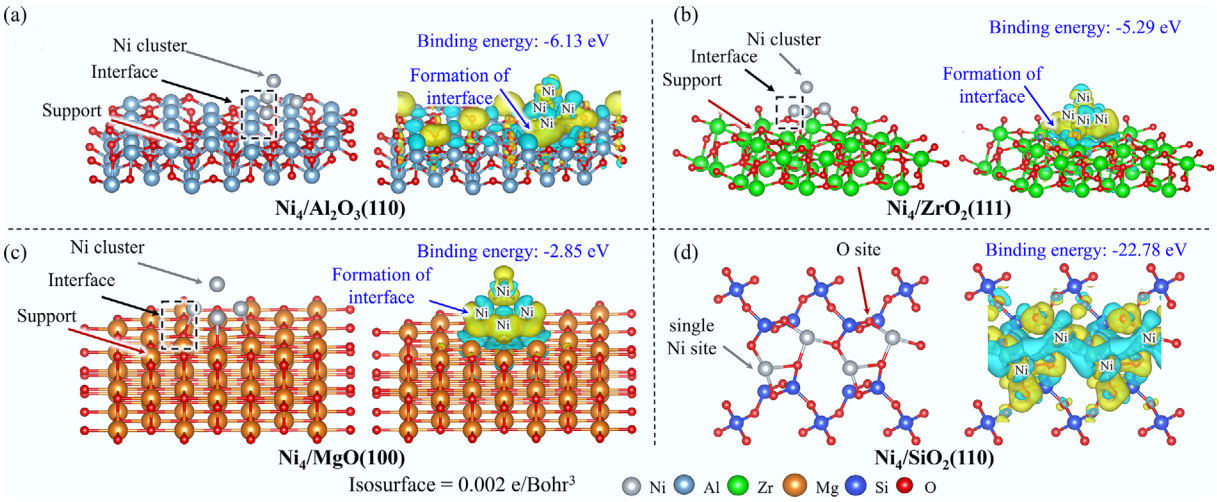

Fig. 1 Theoretical models and the electron transfer between the Ni_4 cluster and substrates.

https://doi.org/10.48130/scm-0026-0018

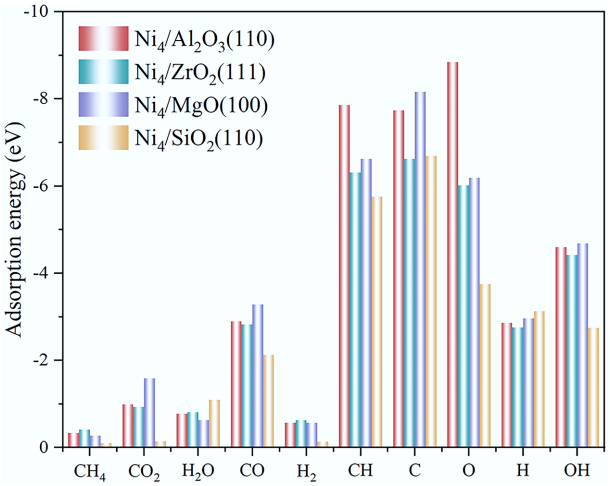

Fig. 2 The adsorption energies of all reaction species on different catalysts.

of CH_4 and the Ni 3d orbitals (Supplementary Fig. S5). Similar adsorption behavior is observed for CH_4 on $Ni_4/ZrO_2(111)$ and $Ni_4/MgO(100)$, where CH_4 stably adsorbs on the Ni_4 cluster with adsorption energies of −0.41 and −0.27 eV, respectively. Notably, in the $Ni_4/MgO(100)$ system, substrate adsorption is also energetically favorable, exhibiting a comparable adsorption energy of −0.28 eV. Consistent with the Al_2O_3 system, electron transfer occurs from the hydrogen atoms of CH_4 to the Ni_4 cluster, with the C 2p and Ni 3d orbitals primarily governing the interfacial interaction. In marked contrast, CH_4 adsorption on $Ni_4/SiO_2(110)$ follows a fundamentally different mechanism, with CH_4 preferentially occupying the Ni site. EDD analysis indicates electron flow from both the Ni atom and the hydrogen atoms of CH_4 into the interfacial region between CH_4 and Ni. However, DOS and COHP analyses reveal negligible interaction between Ni and CH_4, with only weak bonding between the C 2p and Ni 3d orbitals, consistent with the substantially reduced E_{ads} of −0.10 eV.

The adsorption of CH_4 on $Ni_4/ZrO_2(111)$ exhibits the most exothermic behavior among the investigated systems (Fig. 3), with an E_{ads} of −0.41 eV, surpassing those observed for $Ni_4/Al_2O_3(110)$, $Ni_4/MgO(100)$, and $Ni_4/SiO_2(110)$ surfaces. Notably, this adsorption strength also exceeds that on the pristine Ni(111) surface (E_{ads} = −0.33 eV, Supplementary Table S5), indicating that the Ni_4 cluster configuration provides enhanced advantages for CH_4 adsorption processes. Conversely, the markedly weak adsorption of CH_4 on $Ni_4/SiO_2(110)$ (E_{ads} = −0.10 eV) suggests that isolated single Ni atoms do not constitute optimal active sites for methane activation.

On $Ni_4/Al_2O_3(110)$, CO_2 adopts a side-on configuration on the Ni_4 cluster with a substantial E_{ads} of −0.99 eV, wherein two oxygen atoms coordinate with two Ni atoms, resulting in a pronounced bending of the CO_2 molecule to 141°. EDD analysis reveals electron transfer from both the Ni_4 cluster and C atom of CO_2 into the interfacial region between O and Ni, indicative of Ni–O bond formation mediated by hybridization between O 2p and Ni 3d orbitals, as confirmed by DOS analysis (Supplementary Fig. S6). Analogous adsorption phenomena are observed for $Ni_4/ZrO_2(111)$ and $Ni_4/MgO(100)$ systems, where CO_2 similarly adsorbs on the Ni_4 clusters with adsorption energies of −0.93 and −1.59 eV, respectively. Notably, the $Ni_4/MgO(100)$ system demonstrates the most robust CO_2 adsorption, reflected in the most severe CO_2 bending to 134°. EDD mapping corroborates electron redistribution from the Ni_4 cluster and CO_2 toward Ni–O bonds, while DOS and COHP analyses collectively confirm the significant contribution of O 2p and Ni 3d electrons to Ni–O bond formation. In marked contrast, CO_2 interaction with $Ni_4/SiO_2(110)$ is characterized by weak physisorption (E_{ads} = −0.15 eV), wherein CO_2 remains spatially separated from the catalyst surface. Consistent with this minimal interaction, DOS and COHP analyses reveal negligible electronic coupling between Si and CO_2, confirming the absence of significant chemical bonding.

The adsorption behavior of CO_2 demonstrates remarkable consistency across $Ni_4/Al_2O_3(110)$, $Ni_4/ZrO_2(111)$, and $Ni_4/MgO(100)$ systems, wherein CO_2 preferentially adsorbs on the Ni_4 cluster (Fig. 4). Among these systems, $Ni_4/MgO(100)$ exhibits the most thermodynamically favorable adsorption configuration with an E_{ads} of −1.59 eV. Notably, CO_2 undergoes weak physisorption on $Ni_4/SiO_2(110)$ (E_{ads} = −0.15 eV), highlighting the superior efficacy of Ni clusters over isolated Ni atoms for CO_2 adsorption. When compared with the pristine Ni(111) surface (E_{ads} = −0.36 eV), all Ni_4 cluster configurations demonstrate enhanced affinity for CO_2 adsorption. These findings collectively establish Ni clusters as the primary reactive sites for CO_2 adsorption and subsequent activation processes.

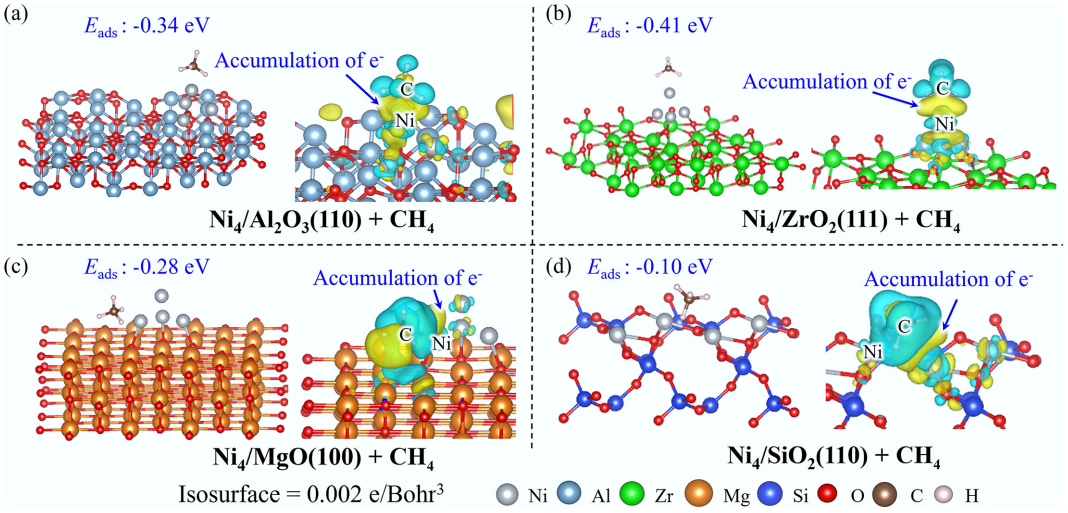

Fig. 3 The most stable adsorption configurations and EDD diagrams of CH_4.

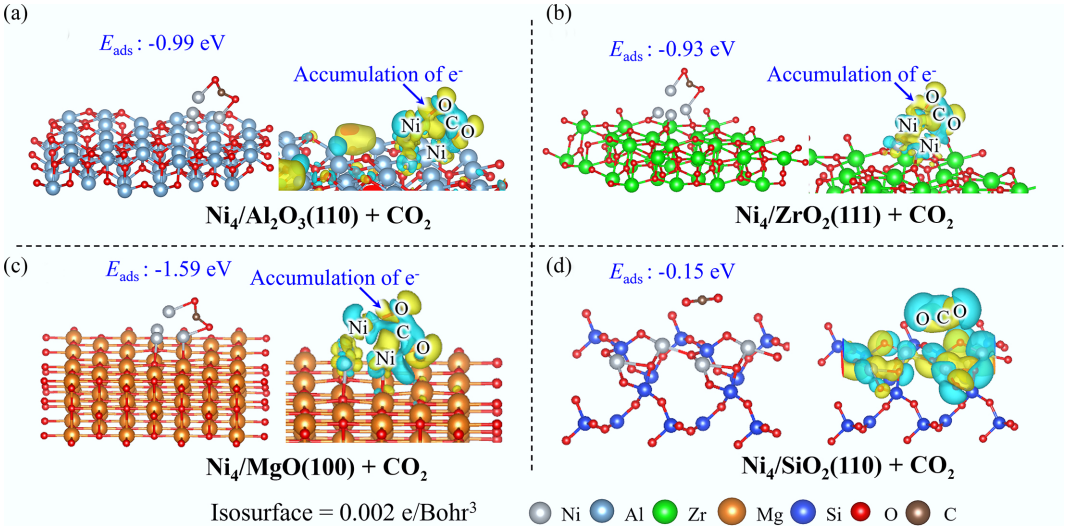

Fig. 4 The most stable adsorption configurations and EDD diagrams of CO_2.

As illustrated in Fig. 5, on $Ni_4/Al_2O_3(110)$, H_2O preferentially adsorbs atop the Ni_4 cluster with a moderate E_{ads} of −0.78 eV, establishing a Ni–O bond with an interatomic distance of 2.01 Å. EDD analysis reveals electron depletion from both H_2O and the Ni_4 cluster toward the Ni–O interfacial region, corroborated by DOS and COHP analyses, which demonstrate significant orbital hybridization between O 2p and Ni 3d states contributing to bond formation (Supplementary Fig. S7). In contrast, on $Ni_4/ZrO_2(111)$ and $Ni_4/MgO(100)$ systems, H_2O preferentially adsorbs on the substrate surfaces, forming robust Zr–O and Mg–O bonds with adsorption energies of −0.81 and −0.63 eV, respectively. Consistent with this substrate-mediated adsorption, electron density accumulation predominantly occurs around the Zr–O/Mg–O bond regions, arising from the hybridization of O 2p electrons with Zr 5s or Mg 3s electrons (Supplementary Fig. S7). Notably, $Ni_4/SiO_2(110)$ exhibits the most thermodynamically favorable H_2O adsorption (E_{ads} = −1.10 eV), wherein H_2O coordinates with Ni atoms to form strong Ni–O bonds.

The adsorption energy hierarchy follows the order $Ni_4/SiO_2(110)$ > $Ni_4/Al_2O_3(110)$ > Ni(111) (E_{ads} = −0.66 eV), indicating a clear preference for H_2O adsorption on isolated atoms and small clusters rather than extended metallic surfaces. Furthermore, the substrate-mediated adsorption behavior observed for $ZrO_2(111)$ and MgO(100) supports suggest a strategic advantage in mitigating H_2O-induced active center sintering, thereby potentially enhancing catalyst stability under steam reforming conditions.

The adsorption of products (CO and H_2)

CO and H_2 are the principal products of methane reforming processes, requiring rapid desorption for sustained catalytic activity to avoid active site poisoning[29].

The adsorption behavior of CO across various catalysts reveals distinct electronic and structural characteristics. On $Ni_4/Al_2O_3(110)$, $Ni_4/ZrO_2(111)$, and $Ni_4/MgO(100)$ surfaces, CO exhibits remarkably similar adsorption configurations, preferentially coordinating to the Ni_4 cluster (Fig. 6). EDD analysis demonstrates significant electron accumulation in the interfacial region between the Ni cluster and CO molecule, indicative of strong metal-adsorbate interactions. Complementary DOS and COHP analyses reveal substantial orbital

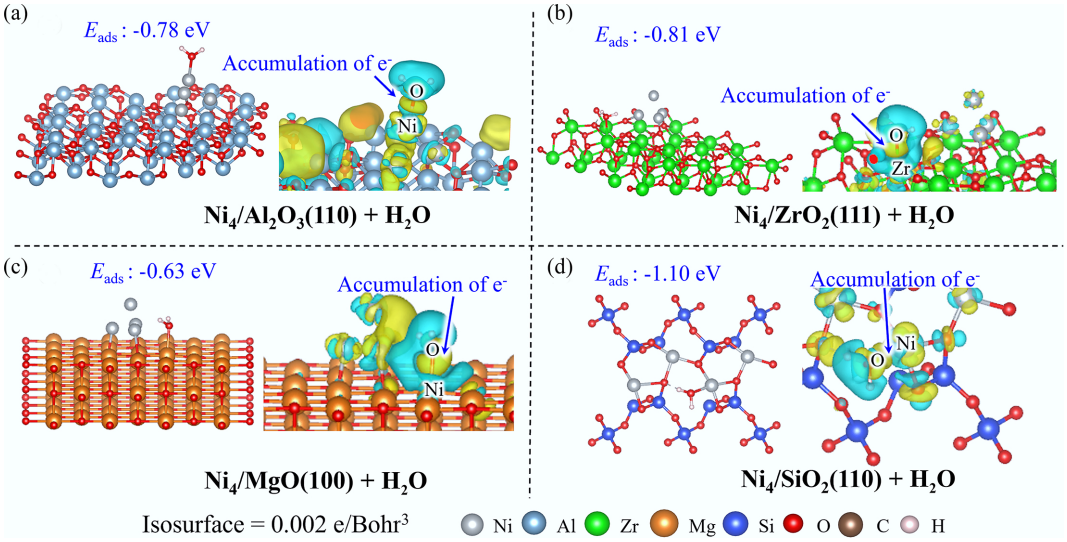

Fig. 5 The most stable adsorption configurations and EDD diagrams of H_2O.

https://doi.org/10.48130/scm-0026-0018

overlap near the Fermi level between Ni and CO, with bonding contributions predominantly arising from the hybridization of C 2p orbitals with Ni 3d/4s orbitals (Supplementary Fig. S8). In contrast, CO adsorption on $Ni_4/SiO_2(110)$ occurs preferentially at the Ni site, where the Ni–C bond formation is mediated through C 2p and Ni 3d electronic interactions.

The thermodynamic hierarchy of CO adsorption energies follows the order: $Ni_4/MgO(100)$ (E_{ads} = −3.29 eV) > $Ni_4/ZrO_2(111)$ (E_{ads} = −2.90 eV) > $Ni_4/Al_2O_3(110)$ (E_{ads} = −2.83 eV) > Ni(111) (E_{ads} = −2.17 eV) > $Ni_4/SiO_2(110)$ (E_{ads} = −2.13 eV). Notably, CO demonstrates a pronounced preference for adsorption on Ni_4 clusters rather than on extended metallic surfaces or isolated atomic sites. Given the exceptionally strong CO adsorption energies observed, particularly on $Ni_4/MgO(100)$, there exists a significant risk of catalyst poisoning through CO over-adsorption, which could potentially compromise the catalytic activity and operational stability of these systems.

The adsorption behavior of H_2 exhibits remarkable uniformity across the investigated supported Ni_4 catalysts (Fig. 7), wherein H_2 preferentially adsorbs atop the Ni_4 cluster in $Ni_4/Al_2O_3(110)$, $Ni_4/ZrO_2(111)$, and $Ni_4/MgO(100)$ configurations, while coordinating to isolated Ni sites in $Ni_4/SiO_2(110)$. EDD analysis reveals significant electron accumulation in the interfacial region between H_2 and the Ni cluster, arising from the hybridization of H 1s and Ni 3d electronic orbitals (Supplementary Fig. S9). Notably, COHP analysis demonstrates that the H_2–Ni interaction in $Ni_4/SiO_2(110)$ is substantially weaker compared with the other catalyst systems.

Consistent with these electronic structure findings, the adsorption energy of H_2 on $SiO_2(110)$ is markedly lower (E_{ads} = −0.14 eV), reflecting its weak interaction strength. For the remaining three supported catalysts, H_2 adsorption energies are comparable (E_{ads} = −0.57 to −0.63 eV) and significantly stronger than that observed on the pristine Ni(111) surface (E_{ads} = −0.25 eV). These findings collectively establish that H_2 exhibits a pronounced preference for adsorption on Ni clusters rather than on extended metallic surfaces or isolated atomic sites, highlighting the enhanced catalytic potential of cluster-based architectures.

The adsorption of key intermediates (CH, C, O, H, and OH)

CH and C intermediates represent critical cracking species in methane reforming, whose adsorption is also a key indicator for carbon

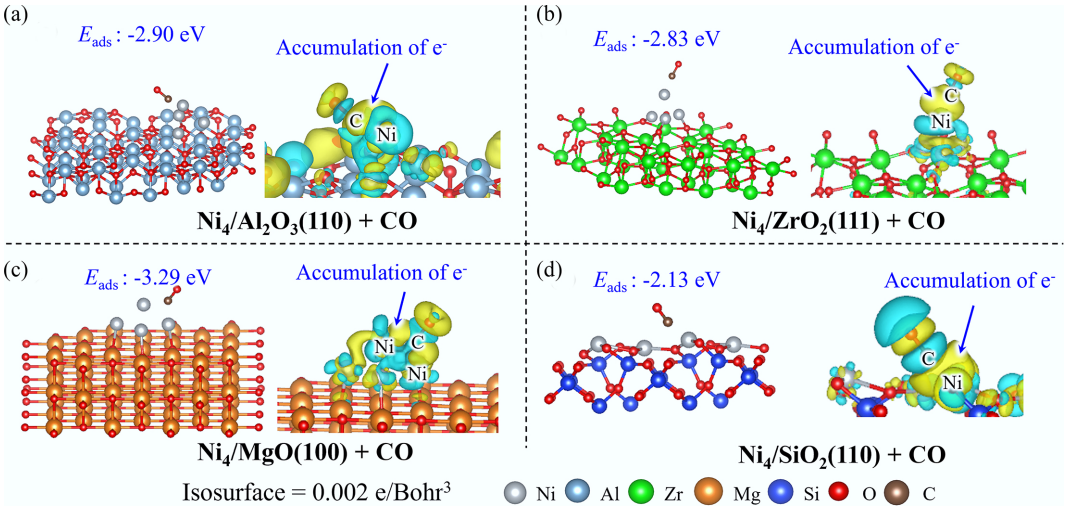

Fig. 6 The most stable adsorption configurations and EDD diagrams of CO.

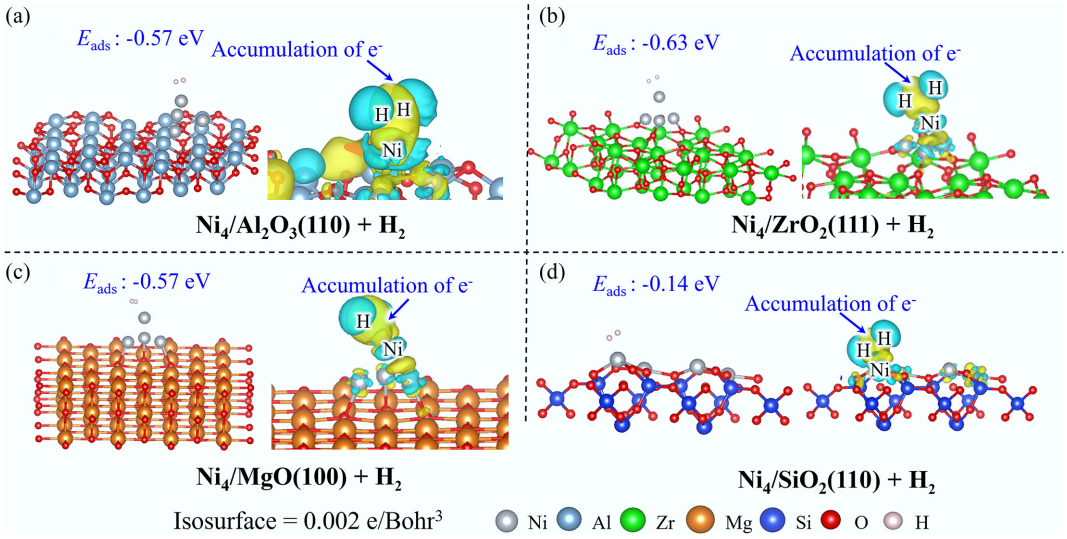

Fig. 7 The most stable adsorption configurations and EDD diagrams of H_2.

deposition. In addition, O, H, and OH groups represent critical secondary surface intermediates throughout the reaction pathway.

Across $Ni_4/Al_2O_3(110)$, $Ni_4/ZrO_2(111)$, and $Ni_4/MgO(100)$ systems, CH intermediates demonstrate preferential interaction with Ni_4 clusters rather than with the substrates (Fig. 8). EDD mapping reveals significant electron accumulation in the interfacial region between Ni clusters and the C atom, indicative of robust Ni–CH interactions (Supplementary Fig. S10). Complementary DOS and COHP analyses demonstrate substantial orbital overlap near the Fermi level between Ni_4 clusters and CH species, with bonding contributions predominantly arising from C 2p and Ni 3d orbital hybridization. In contrast, CH exhibits dual-site interaction with $Ni_4/SiO_2(110)$, simultaneously coordinating with both the Ni atom and surface oxygen atoms. Electronic structure analysis indicates electron depletion from Ni and O atoms toward the Ni–CH interfacial region, mediated through Ni 3d and C 2p orbital overlap (Supplementary Fig. S10).

Thermodynamic analysis of adsorption strengths reveals that the interaction between CH and $Ni_4/Al_2O_3(110)$ exhibits the highest binding affinity (E_{ads} = −7.86 eV), consistent with the strong orbital interactions evidenced by COHP analysis. This adsorption energy substantially exceeds that of CH on the pristine Ni(111) surface (E_{ads} = −6.76 eV), while other catalyst systems demonstrate moderate binding strengths (E_{ads} = −5.76 to −6.62 eV). Notably, the adsorption energy of CH on $Ni_4/SiO_2(110)$ is significantly diminished compared with other catalysts, highlighting the superior affinity of Ni clusters and bulk metallic surfaces for CH intermediates relative to isolated Ni sites.

The adsorption behavior of C atoms across different catalyst systems reveals distinct structural and electronic characteristics that govern catalyst–carbon interactions. On $Ni_4/Al_2O_3(110)$, C adsorption induces significant reconstruction of the Ni_4 cluster, wherein the C atom simultaneously coordinates with four Ni atoms (Fig. 8). EDD analysis demonstrates substantial electron accumulation in the interfacial region between the C atom and Ni_4 cluster, while DOS and COHP analyses reveal pronounced orbital overlap between Ni 3d and C 2p orbitals, indicating a robust interaction (Supplementary Fig. S11). Analogous adsorption phenomena are observed for $Ni_4/ZrO_2(111)$ and $Ni_4/MgO(100)$ systems, where the C atom interacts with Ni_4 clusters that maintain their structural integrity without significant distortion. Similar electron accumulation patterns emerge in the Ni–C interfacial regions, mediated through C 2p and Ni 3d orbital hybridization. In contrast, the $Ni_4/SiO_2(110)$ system exhibits distinctive adsorption behavior, wherein the C atom simultaneously coordinates with both surface Ni and O atoms, forming Ni–C and C–O bonds with interatomic distances of 1.25 and 1.65 Å, respectively. The Ni–C interaction predominates in this system, with electronic contributions arising from the C 2p and Ni 3d orbital overlap.

Thermodynamic analysis of adsorption strengths reveals a clear hierarchy: $Ni_4/MgO(100)$ demonstrates the most stable carbon adsorption (E_{ads} = −8.16 eV), followed by $Ni_4/Al_2O_3(110)$ (E_{ads} =

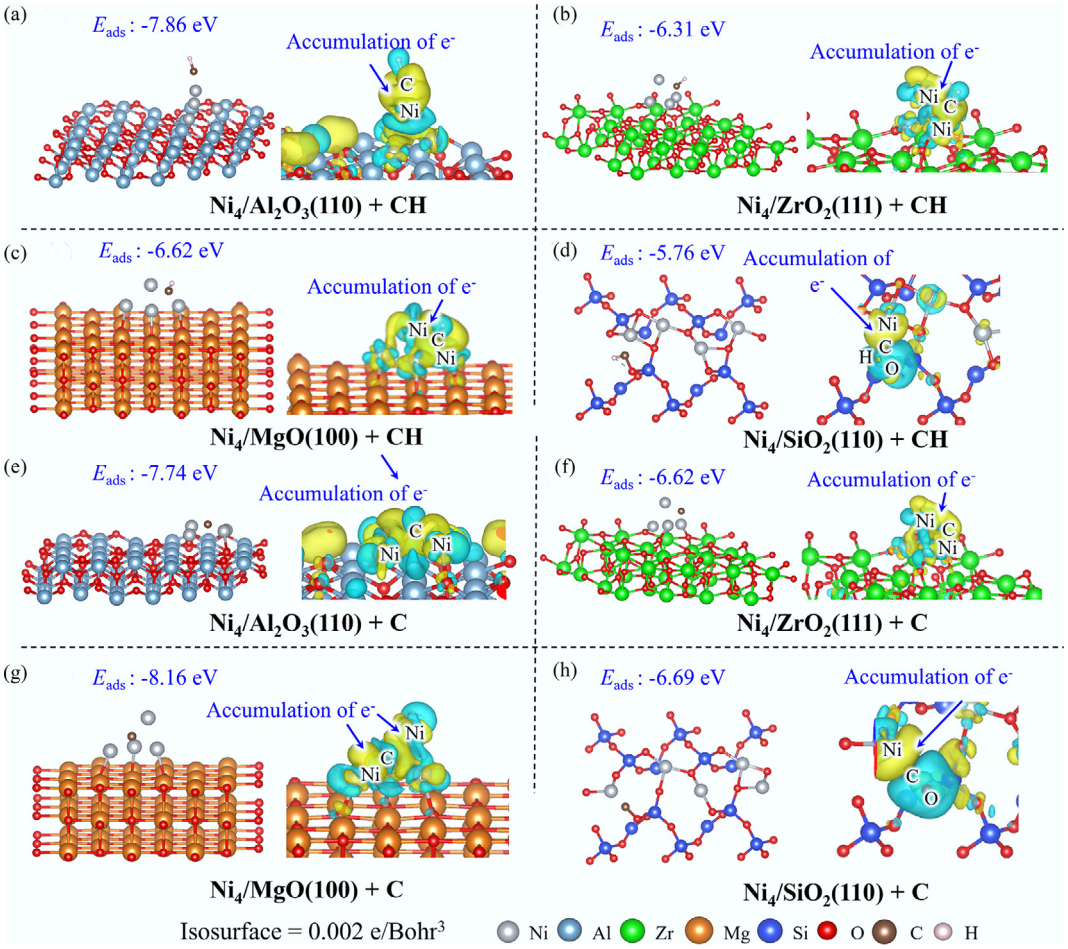

Fig. 8 The most stable adsorption configurations and EDD diagrams of (**a**)–(**d**) CH, and (**e**)–(**h**) C.

https://doi.org/10.48130/scm-0026-0018

−7.74 eV). Both systems exhibit substantially stronger C affinity compared with the pristine Ni(111) surface (E_{ads} = −7.11 eV). Conversely, $Ni_4/ZrO_2(111)$ (E_{ads} = −6.62 eV) and $Ni_4/SiO_2(110)$ (E_{ads} = −6.69 eV) demonstrate relatively weaker carbon binding capabilities, highlighting the critical role of support materials in modulating the catalyst–carbon interaction.

On $Ni_4/Al_2O_3(110)$ and $Ni_4/ZrO_2(111)$ surfaces, oxygen species preferentially adsorb on the substrate, forming robust Al–O or Zr–O bonds that induce significant surface electronic structure reconstruction (Fig. 9). DOS and COHP analyses elucidate that these interactions predominantly arise from orbital hybridization between O 2p and Al 3p or Zr 4d orbitals (Supplementary Fig. S12). In contrast, on Ni_4/MgO(100), O adsorption occurs at the sublayer of the Ni_4 cluster, with electrons flowing from the Ni_4 cluster into the interfacial region between O and the metallic cluster. Both DOS and COHP analyses confirm the substantial contribution of Ni 3d and O 2p orbitals to these metal–oxygen interactions. Distinctively, oxygen adsorption on $Ni_4/SiO_2(110)$ results in the formation of a Ni–O–Ni bridge structure, wherein both Ni–O interactions are mediated through Ni 3d and O 2p orbital hybridization.

Thermodynamic analysis reveals that O adsorption on $Ni_4/Al_2O_3(110)$ exhibits the strongest binding (E_{ads} = −8.85 eV), reflecting the pronounced oxygen affinity of aluminum species. The O adsorption on Ni_4/MgO(100) and $Ni_4/ZrO_2(111)$ demonstrates moderate binding strengths with adsorption energies of −6.19 and −6.02 eV, respectively. Notably, all these systems display superior O

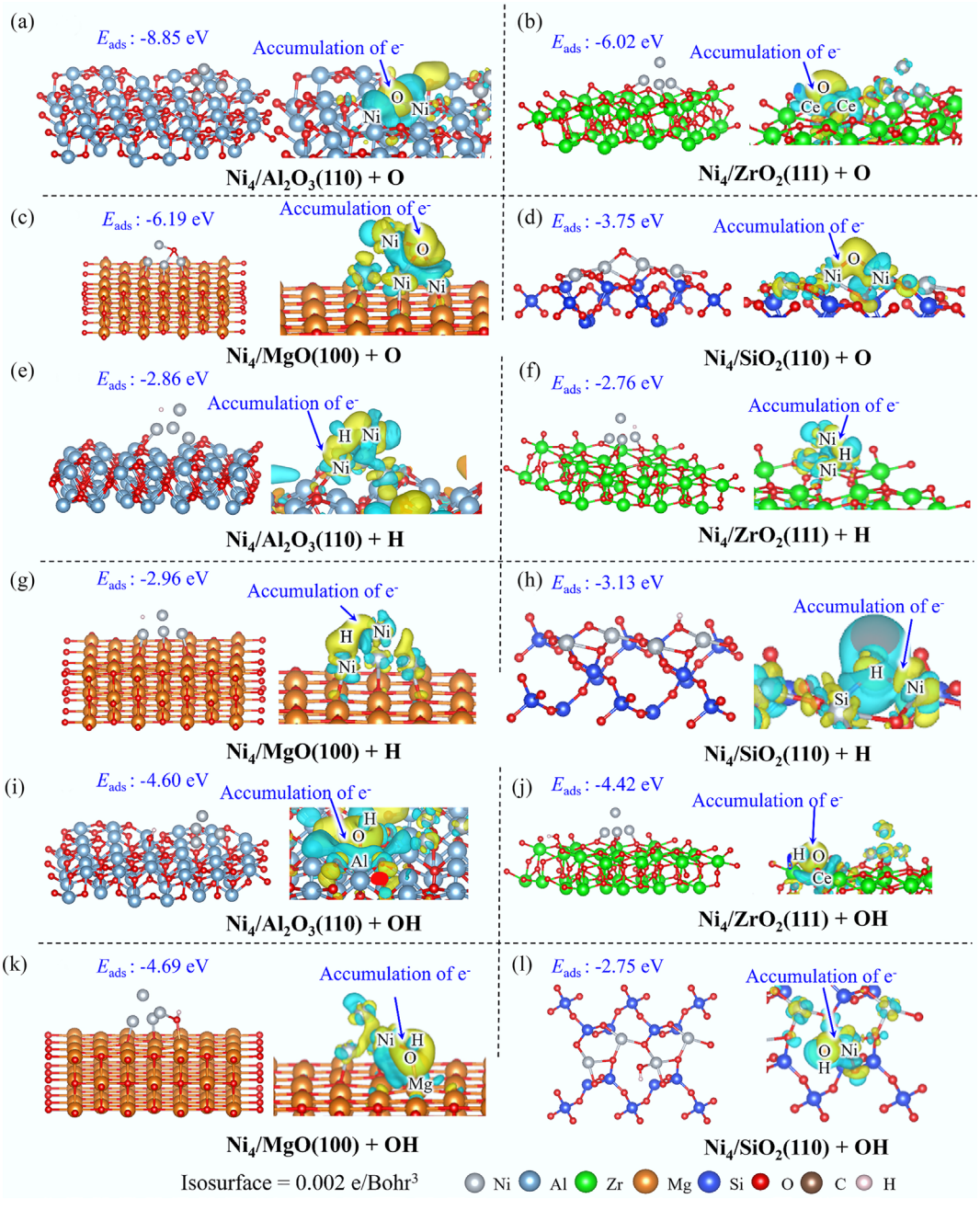

Fig. 9 The most stable adsorption configurations and EDD diagrams of (**a**)–(**d**) O, (**e**)–(**h**) H, and (**i**)–(**l**) OH.

affinity compared with the pristine Ni(111) surface (E_{ads} = −5.95 eV), with the exception of $Ni_4/SiO_2(110)$, which exhibits significantly weaker O adsorption (E_{ads} = −3.75 eV). These findings collectively demonstrate that O adsorption is highly sensitive to the supports, with a clear tendency for oxygen to preferentially adsorb on hydrophilic substrates such as Al_2O_3 rather than on the metallic active sites.

On $Ni_4/Al_2O_3(110)$, $Ni_4/ZrO_2(111)$, and Ni_4/MgO(100), H preferentially adsorbs on the Ni_4 cluster driven by nickel's high hydrogen affinity (Fig. 9). EDD, DOS, and COHP analyses collectively reveal significant electron accumulation in the interfacial region between the H atom and the Ni_4 cluster, with interactions predominantly arising from H 1s and Ni 3d orbital hybridization (Fig. 9 and Supplementary Fig. S13). In contrast, on $Ni_4/SiO_2(110)$, H preferentially adsorbs on substrate oxygen atoms, resulting in O–H bond formation with interactions primarily mediated through O 2p and H 1s orbital overlap.

Thermodynamic analysis demonstrates that H adsorption on $Ni_4/SiO_2(110)$ exhibits the highest stability (E_{ads} = −3.13 eV), marginally exceeding that on the pristine Ni(111) surface (E_{ads} = −3.07 eV). Conversely, H adsorption on $Ni_4/Al_2O_3(110)$, Ni_4/MgO(100), and $Ni_4/ZrO_2(111)$ demonstrates reduced binding strength compared with Ni(111), with adsorption energies of −2.89, −2.96, and −2.76 eV, respectively. These findings indicate a slight preference for H interacting with bulk Ni(111) surfaces over dispersed clusters, albeit the energetic differences are minimal.

The adsorption behavior of OH also exhibits distinct substrate-dependent interactions. On $Ni_4/Al_2O_3(110)$ and $Ni_4/ZrO_2(111)$, OH species preferentially adsorb on the substrate surfaces, establishing interactions with metal atoms through electron transfer from OH and Al/Zr species into Al/Zr–O bonds (Fig. 9). These interactions are predominantly mediated through orbital hybridization between O 2p and Al 3p or Zr 4d states (Supplementary Fig. S14). In contrast, OH adsorption on Ni_4/MgO(100) occurs preferentially at the interfacial region, where significant electron accumulation is observed, and O 2p and Ni 3d orbitals contribute substantially to these metal-adsorbate interactions. Distinctively, on $Ni_4/SiO_2(110)$, OH coordinates directly with Ni atoms, forming Ni–O bonds through the hybridization of O 2p and Ni 3d orbitals, as evidenced by EDD, DOS, and COHP analyses.

Thermodynamic analysis of adsorption strengths reveals that OH adsorption on Ni_4/MgO(100) exhibits the most exothermic (E_{ads} = −4.69 eV), reflecting the exceptionally strong interaction intensity between the interfacial site and OH. Concurrently, OH demonstrates robust adsorption on $Al_2O_3(110)$ and $ZrO_2(111)$, with adsorption energies of −4.60 and −4.42 eV, respectively; both substantially exceeding that observed on the pristine Ni(111) surface (E_{ads} = −3.74 eV). Exceptionally, OH interaction with the Ni atom in $Ni_4/SiO_2(110)$ releases only 2.75 eV of energy, indicating the relatively weak affinity of isolated Ni atomic sites for OH species compared with cluster-based configurations.

Discussion

The reactivity of different supported catalysts

Different supports profoundly influence the catalytic performance of Ni_4 clusters for methane reforming. Different supports influence both adsorption sites and energies, and the adsorption strength order is summarized in Supplementary Table S7.

Carbon-containing species (CH_4, CO_2, CO, CH, and C) and H species (H/H_2) preferentially adsorb on the Ni_4 cluster of $Ni_4/Al_2O_3(110)$, $Ni_4/ZrO_2(111)$, and Ni_4/MgO(100), indicating that the complete methane dry reforming process ($CH_4 + CO_2 \rightarrow 2CO + 2H_2$) can proceed entirely on the active Ni_4 cluster. Conversely, O-containing species (O, OH, and H_2O) exhibit a strong affinity for the substrate due to the superior oxygen-binding capability of support metals compared to Ni, enabling substrates to participate in steam reforming as H_2O adsorption sites. $Ni_4/SiO_2(110)$ represents a distinctive case, where most reaction species adsorb on isolated Ni sites.

Compared to the Ni(111) surface, supported Ni_4 clusters on $Al_2O_3(110)$, $ZrO_2(111)$, and MgO(100) carriers exhibit significantly enhanced adsorption energies for all species. In particular, $Ni_4/Al_2O_3(110)$ exhibits substantially increased adsorption energies for C, CH, and O species by about 0.6, 1.1, and 2.8 eV, respectively, leading to the promoted deep cracking activity. $Ni_4/ZrO_2(111)$ also demonstrates generally elevated adsorption energies for all species, especially for reactants (CH_4, CO_2, and H_2O), indicating that ZrO_2 can facilitate the reaction by enhancing the interaction between the Ni_4 cluster and reactants. Similarly, Ni_4/MgO(100) displays markedly increased adsorption energies for most species, with OH, C, and CO_2 exhibiting increases exceeding 1 eV. In contrast, the Ni_4 cluster disperses into isolated single-atom sites on $SiO_2(110)$, resulting in diminished adsorption energies, except for H_2O adsorption. Consequently, SiO_2 support fails to improve Ni activity and may promote H_2O-induced sintering due to the strengthened Ni–H_2O interactions[30].

Quantitatively, the adsorption strength of CH_4, CO_2, and H_2O on $Ni_4/Al_2O_3(110)$, $Ni_4/ZrO_2(111)$, and Ni_4/MgO(100) is comparable (E_{ads} = −0.28 to −0.41 eV, and −0.93 to −1.59 eV), substantially higher than those on the Ni(111) surface (−0.33 eV and −0.36 eV) and $Ni_4/SiO_2(110)$ (−0.10 eV and −0.15 eV). Notably, MgO exhibits exceptional CO_2 adsorption capabilities, which substantially enhances dry reforming activity. This promotional effect is corroborated by experimental evidence where Jin et al.[31] reported a 26% increase in methane dry reforming conversion at 850 °C upon MgO doping into Ni/Al_2O_3 catalysts, underscoring the critical role of basic oxide supports in facilitating CO_2 activation. For deep CH_4 dissociation intermediates (C/CH), the sequence is MgO (−8.16/−6.62 eV) > Al_2O_3 (−7.74/−7.86 eV) > ZrO_2 (−6.62/−6.31 eV) > SiO_2 (−6.69/−5.76 eV). The exceptionally strong adsorption on MgO and Al_2O_3 facilitates complete methane cracking, consistent with prior studies where MgO doping enhanced dry reforming via strengthened SMSI[32]. However, for the adsorption of CO, the sequence is MgO (−3.29 eV) > Al_2O_3 (−2.90 eV) > ZrO_2 (−2.83 eV) > SiO_2 (−2.13 eV). Notably, MgO exhibits the strongest affinity toward both CO and CO_2 among the investigated supports, which may also lead to active-site poisoning. This observation aligns with the Sabatier principle that excessively strong adsorption of reactants can impede product desorption, thereby compromising catalytic performance. This also highlights a critical trade-off: while stronger adsorption of reactants/intermediates is beneficial, excessive CO adsorption can lead to active site poisoning and reaction inhibition[29].

Furthermore, reaction kinetics govern the overall catalytic performance. Reported literature identifies C–H bond activation as the rate-determining step for methane reforming, particularly under high-temperature conditions[33]. Accordingly, we evaluated the activation barriers for CH_4 dissociation across the four supported Ni_4 clusters (Supplementary Fig. S15). The calculated energy barriers follow the sequence: $Ni_4/Al_2O_3(110)$ (0.397 eV) ≈ Ni_4/MgO(100) (0.400 eV) < $Ni_4/ZrO_2(111)$ (0.588 eV) < $Ni_4/SiO_2(110)$ (1.170 eV). This kinetic hierarchy indicates superior catalytic activity for Al_2O_3- and MgO-supported systems, corroborating both the thermodynamic predictions and experimental observations that Ni/Al_2O_3

https://doi.org/10.48130/scm-0026-0018

outperforms Ni/ZrO_2 and Ni/SiO_2[34], while MgO doping further enhances catalytic turnover[31].

In summary, Ni_4 supported on MgO, Al_2O_3, and ZrO_2 supports generally exhibits promoted intrinsic reactivity by strengthening the adsorption of reactants and cracking intermediates.

Carbon deposition and elimination

The Sabatier principle also provides a fundamental framework for understanding carbon deposition resistance. Carbon adsorption energy serves as the fundamental descriptor governing carbon deposition propensity on supported Ni catalysts. According to the foregoing analysis, atomic C exhibits exceptionally strong binding on Ni_4/MgO(100), with an adsorption energy of −8.16 eV. According to the Sabatier principle, such excessive adsorption strength implies a substantial kinetic barrier for carbon removal or further conversion to gaseous products. Hence, this pronounced binding renders deposited carbon thermodynamically and kinetically trapped. Consistent with this, Zhang et al.[35] reported that deep cracking products of CH_4 on MgO-supported catalysts exhibit limited removability, indicating inferior resistance to carbon deposition. This suggests that, despite the promotional effect of MgO on CO_2 activation, its inadequate capability for carbon elimination may compromise long-term catalytic stability. The availability of active oxygen species represents another crucial factor governing carbon elimination through the $C^* + O^* \rightarrow CO^*$ pathway. Although C is also strongly adsorbed on Al_2O_3(110) support surface (E_{ads} = −7.74 eV), Al_2O_3(110) also demonstrates remarkable capability to stably adsorb oxygen atoms with exceptionally high binding energy (E_{ads} = −8.85 eV), effectively creating a rich 'oxygen reservoir' that facilitates carbon removal. In contrast, ZrO_2(111) exhibits a more balanced profile with moderate carbon adsorption strength (E_{ads} = −6.62 eV) coupled with strong oxygen affinity (E_{ads} = −6.02 eV), resulting in superior resistance to carbon deposition, in agreement with experimental findings[36–38]. Ni_4/SiO_2(110) presents an interesting case study, displaying carbon adsorption intensity comparable to ZrO_2(111) (E_{ads} = −6.69 eV), yet significantly weaker oxygen affinity (E_{ads} = −3.75 eV), exhibiting a stronger tendency toward carbon deposition. These theoretical predictions are corroborated by experimental studies. Xu et al.[39] demonstrated the inferior stability of Ni/SiO_2 relative to Ni/Al_2O_3, attributing this to the enhanced carbon deposition propensity. Meanwhile, Pizzolitto et al.[34] established a stability hierarchy of Ni/Al_2O_3 > Ni/ZrO_2/Ni/SiO_2 under reaction conditions. Furthermore, Zhang et al.[40] revealed that carbonaceous deposits on Ni/ZrO_2 exhibit superior reactivity toward CO_2 oxidation at lower temperatures compared with those on Ni/SBA-15, indicating the enhanced carbon resistance of ZrO_2 supports. Collectively, these findings establish the following trend in anti-coking performance: $Al_2O_3 \approx ZrO_2 > SiO_2$. This comparative analysis reveals the delicate balance between carbon binding strength and oxygen availability in determining overall catalyst stability.

From the perspective of carbon deposition resistance, ZrO_2 emerges as the optimal support, offering an ideal compromise between moderate carbon adsorption and sufficient oxygen supply for effective carbon removal. This balanced approach ensures sustained catalytic activity while minimizing carbon accumulation.

Summary

Figure 10 presents a comprehensive comparison of oxide support effects on Ni-catalyzed methane reforming. Ni_4/Al_2O_3(110) exhibits superior catalytic performance, attributable to its optimal adsorption of reaction intermediates, facile C–H bond activation, and strong oxygen affinity that promotes carbon removal via CO formation. Ni_4/ZrO_2(111) similarly demonstrates excellent activity, with balanced carbon and

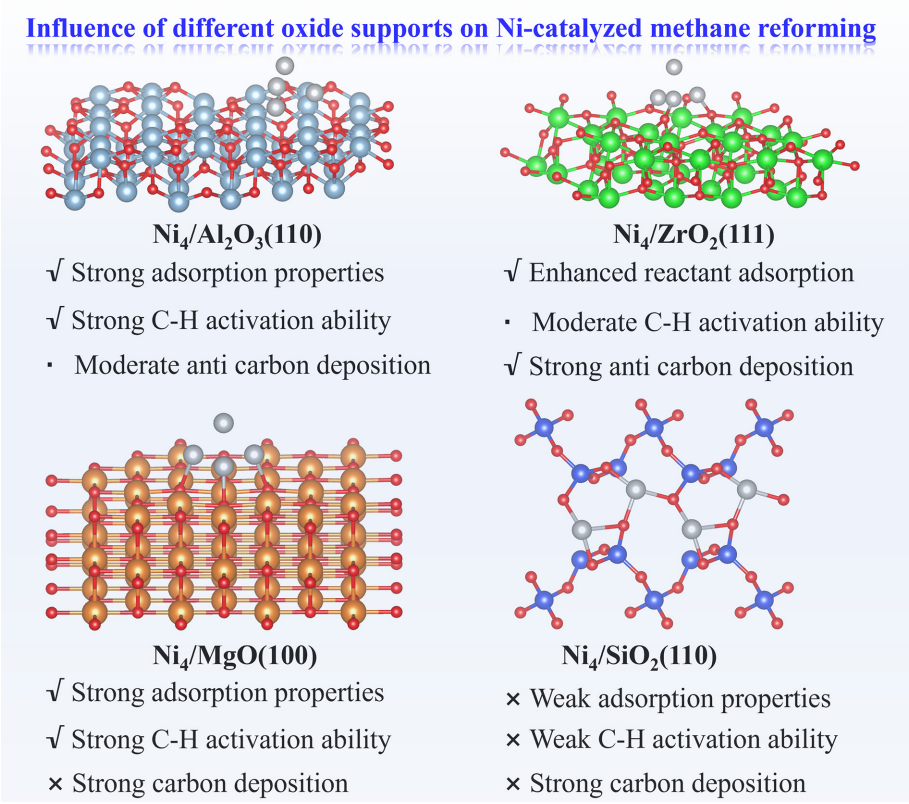

Fig. 10 The influence of different substrates on Ni-catalyzed methane reforming.

oxygen adsorption energetics that effectively suppress coking. In contrast, Ni_4/MgO(100) displays high intrinsic activity, but suffers from excessive binding of atomic C and CO, leading to severe carbon deposition and active site poisoning that compromises operational stability. Finally, Ni_4/SiO_2(110) exhibits both low catalytic activity and pronounced carbon deposition propensity.

Conclusions

The present study elucidates the profound influence of different oxide supports on the catalytic performance of Ni-based catalysts in methane reforming, through systematic DFT calculations. By examining the adsorption behavior of reactants, key intermediates, and products across various supported catalyst systems, the fundamental structure-activity relationships that guide catalyst design optimization are established.

Comparative analysis reveals that supported Ni catalysts generally exhibit superior reactivity for methane reforming compared with the bulk Ni(111) surface. Cluster-based catalysts, including Ni_4/Al_2O_3(110), Ni_4/ZrO_2(111), and Ni_4/MgO(100), demonstrate highly consistent adsorption behavior for reactants (CH_4, CO_2, and H_2O), indicating universal enhancement mechanisms across different oxide supports.

Distinctively, Al_2O_3(110) and MgO(100) supports significantly enhance reaction thermodynamics and exhibit strong reaction activity, as evidenced by the increased adsorption energies of C/CH and CO species, as well as their low C–H activation energy barrier. However, the strong adsorption of carbon-containing species also increases the risk of carbon deposition and potential active site poisoning by CO, especially for MgO(100), representing a classic activity-stability dilemma. ZrO_2 emerges as a particularly promising support, by offering moderate enhancement of Ni_4 cluster activity while simultaneously reducing carbon deposition tendencies. This balanced approach provides an effective strategy for addressing the fundamental activity-stability trade-off that plagues conventional Ni-based catalysts. In addition, Ni_4/SiO_2(110) exhibits relatively weak reactivity, although it is important to note that this system cannot represent the full spectrum of Si-based supported catalysts.

The development of composite catalysts that precisely control the distribution of active components while optimizing the anti-carbon deposition properties of substrates remains a crucial research priority. Such rational design strategies hold the key to breaking the long-standing activity-stability trade-off and enabling next-generation methane reforming catalysts with unprecedented performance and durability.

Supplementary information

It accompanies this paper at: https://doi.org/10.48130/scm-0026-0018.

Author contributions

The authors confirm their contributions to the paper as follows: Yuangu Xia: investigation, methodology, formal analysis, writing – original draft; Haoyu Wang: investigation, methodology, formal analysis; Bin Hu: conceptualization, writing – revised draft, funding acquisition; Huaide Sun: investigation, review – revised draft; Tahir Iqbal: investigation, methodology; Ji Liu: conceptualization, writing – revised draft, funding acquisition; Qiang Lu: supervision, writing – revised draft, funding acquisition. All authors reviewed the results and approved the final version of the manuscript.

Data availability

The datasets generated during and analyzed during the current study are available from the corresponding author on reasonable request.

Funding

This work was supported by the National Natural Science Foundation of China (Grant Nos 52376182 and 52436009) and the Fundamental Research Funds for the Central Universities (Grant No. 2024JG003).

Declarations

Competing interests

The authors declare that they have no known competing financial interests or personal relationships that could have appeared to influence the work reported in this paper.

Author details

[1]National Engineering Research Center of New Energy Power Generation, North China Electric Power University, Beijing 102206, China; [2]Faculty of Agricultural Engineering and Technology, PMAS-Arid Agriculture University Rawalpindi, Rawalpindi 46000, Pakistan

References

[1] Sun Z, Liao Y, Zhang Y, Sun S, Kan Q, et al. 2025. Sustainable carbon materials in environmental and energy applications. *Sustainable Carbon Materials* 1:e007

[2] Liu Z, Li J, Buettner M, Ranganathan RV, Uddi M, et al. 2019. Metal–support interactions in CeO_2- and SiO_2-supported cobalt catalysts: effect of support morphology, reducibility, and interfacial configuration. *ACS Applied Materials & Interfaces* 11:17035–17049

[3] Han J, Yang J, Zhang Z, Jiang X, Liu W, et al. 2023. Strong metal–support interaction facilitated multicomponent alloy formation on metal oxide support. *Journal of the American Chemical Society* 145:22671–22684

[4] Jeon OS, Lee H, Lee KS, Paidi VK, Ji Y, et al. 2022. Harnessing strong metal–support interaction to proliferate the dry reforming of methane performance by *in situ* reduction. *ACS Applied Materials & Interfaces* 14:12140–12148

[5] Pu T, Zhang W, Zhu M. 2023. Engineering heterogeneous catalysis with strong metal–support interactions: characterization, theory and manipulation. *Angewandte Chemie International Edition* 62:e202212278

[6] Wang F, Pace R, Ji Y, Jiang J, Jiang X, et al. 2022. Effect of Pd promotion and catalyst support on the Ni-catalyzed deoxygenation of tristearin to fuel-like hydrocarbons. *Renewable Energy* 195:1468–1479

[7] Luo Z, Zhao G, Pan H, Sun W. 2022. Strong metal–support interaction in heterogeneous catalysts. *Advanced Energy Materials* 12:2201395

[8] Wu P, Tan S, Moon J, Yan Z, Fung V, et al. 2020. Harnessing strong metal–support interactions via a reverse route. *Nature Communications* 11:3042

[9] Hou Z, Cui C, Yang Y, Huang Z, Zhuang Y, et al. 2024. Strong metal-support interactions in heterogeneous oxygen electrocatalysis. *Small* 20:2407167

[10] Wang Y, Zhu S, Lu J, Liu J, Zhao Y, et al. 2022. Boosting hydrogen production from steam reforming of glycerol via constructing moderate metal-support interaction in Ni@Al_2O_3 catalyst. *Fuel* 324:124583

[11] Chen H, Bai W, He Y, Pfefferle LD, Qi S, et al. 2018. Catalytic hydrogenation of octanoic acid in the gaseous phase on Ni catalysts: the effect of support species and structure. *Industrial & Engineering Chemistry Research* 57:16272–16283

[12] Mierczynski P, Mosinska M, Stepinska N, Chalupka K, Nowosielska M, et al. 2021. Effect of the support composition on catalytic and physicochemical properties of Ni catalysts in oxy-steam reforming of methane. *Catalysis Today* 364:46–60

[13] Zhao W, Fu Q, Xie B, Ni Z, Xia S. 2024. Mechanistic study of transition metal loaded/doped Ni–MgO catalyzed dry reforming of methane: DFT calculations. *Chemical Physics Letters* 853:141538
[14] Lee J, Jang EJ, Oh DG, Szanyi J, Kwak JH. 2020. Morphology and size of Pt on Al_2O_3: the role of specific metal-support interactions between Pt and Al_2O_3. *Journal of Catalysis* 385:204–212
[15] Yang X, Meng Q, Ding G, Wang Y, Chen H, et al. 2018. Construction of novel Cu/ZnO-Al_2O_3 composites for furfural hydrogenation: the role of Al components. *Applied Catalysis A: General* 561:78–86
[16] Gao M, Zhang J, Zhu P, Liu X, Zheng Z. 2022. Unveiling the origin of alkali metal promotion in CO_2 methanation over Ru/ZrO_2. *Applied Catalysis B: Environmental* 314:121476
[17] Han A, Ding J, Zhong Q. 2022. Role of single-atom Pd in Cu/ZrO_2 catalysts for CO_2 hydrogenation to methanol. *Colloids and Surfaces A: Physicochemical and Engineering Aspects* 641:128535
[18] Lee K, Woo R, Woo HC, Ko G, Cho K, et al. 2024. Unraveling the role of MgO in the Ru-Ba/MgO catalyst for boosting ammonia synthesis: comparative study of MgO and $MgAlO_x$ supports. *Journal of Catalysis* 434:115530
[19] Liu J, Li C, Niu H, Liang C. 2022. Role of metal (Pt)–support (MgO) interactions in base-free glucose dehydrogenation. *Catalysis Science & Technology* 12:6849–6855
[20] Javaid R, Nanba T. 2023. Efficient Ru/MgO–CeO_2 catalyst for ammonia synthesis as a hydrogen and energy carrier. *International Journal of Hydrogen Energy* 48:11214–11224
[21] Lombard CJ, van Sittert CGCE, Mugo JN, Perry C, Willock DJ. 2023. Computational investigation of α-SiO_2 surfaces as a support for Pd. *Physical Chemistry Chemical Physics* 25:6121–6130
[22] Gosavi A, Mirkin C, Notestein J. 2020. Mapping the thermal entrenchment behavior of Pd nanoparticles on planar SiO_2 supports. *Nanoscale* 12:14245–14258
[23] Wang HY, Ruckenstein E. 2000. Carbon dioxide reforming of methane to synthesis gas over supported rhodium catalysts: the effect of support. *Applied Catalysis A: General* 204:143–152
[24] Drummond ML, Sumpter BG, Shelton WA, Larese JZ. 2007. Electronic structure investigation of surface–adsorbate and adsorbate–adsorbate interactions in multilayers of CH_4 on MgO(100). *The Journal of Physical Chemistry C* 111:966–976
[25] Kresse G, Joubert D. 1999. From ultrasoft pseudopotentials to the projector augmented-wave method. *Physical Review B* 59:1758–1775
[26] Doust Mohammadi M, Abdullah HY, Kalamse V, Chaudhari A. 2022. Bromochlorodifluoromethane interaction with pristine and doped BN nanosheets: a DFT study. *Journal of Environmental Chemical Engineering* 10:108367
[27] Momma K, Izumi F. 2011. VESTA 3 for three-dimensional visualization of crystal, volumetric and morphology data. *Journal of Applied Crystallography* 44:1272–1276
[28] Wang V, Xu N, Liu JC, Tang G, Geng WT. 2021. VASPKIT: a user-friendly interface facilitating high-throughput computing and analysis using VASP code. *Computer Physics Communications* 267:108033
[29] Araújo TP, Morales-Vidal J, Giannakakis G, Mondelli C, Eliasson H, et al. 2023. Reaction-induced metal-metal oxide interactions in Pd-In_2O_3/ZrO_2 catalysts drive selective and stable CO_2 hydrogenation to methanol. *Angewandte Chemie International Edition* 62:e202306563
[30] Prašnikar A, Pavlišič A, Ruiz-Zepeda F, Kovač J, Likozar B. 2019. Mechanisms of copper-based catalyst deactivation during CO_2 reduction to methanol. *Industrial & Engineering Chemistry Research* 58:13021–13029
[31] Jin B, Li S, Liang X. 2021. Enhanced activity and stability of MgO-promoted Ni/Al_2O_3 catalyst for dry reforming of methane: role of MgO. *Fuel* 284:119082
[32] Shi C, Zhang P. 2015. Role of MgO over γ-Al_2O_3-supported Pd catalysts for carbon dioxide reforming of methane. *Applied Catalysis B: Environmental* 170–171:43–52
[33] Yu YX, Yang J, Zhu KK, Sui ZJ, Chen D, et al. 2021. High-throughput screening of alloy catalysts for dry methane reforming. *ACS Catalysis* 11:8881–8894
[34] Pizzolitto C, Pupulin E, Menegazzo F, Ghedini E, Di Michele A, et al. 2019. Nickel based catalysts for methane dry reforming: effect of supports on catalytic activity and stability. *International Journal of Hydrogen Energy* 44:28065–28076
[35] Zhang L, Li L, Li J, Zhang Y, Hu J. 2014. Carbon dioxide reforming of methane over nickel catalyst supported on MgO(111) nanosheets. *Topics in Catalysis* 57:619–626
[36] Therdthianwong S, Siangchin C, Therdthianwong A. 2008. Improvement of coke resistance of Ni/Al_2O_3 catalyst in CH_4/CO_2 reforming by ZrO_2 addition. *Fuel Processing Technology* 89:160–168
[37] Abahussain AAM, Al-Fatesh AS, Singh SK, Almutairi G, Fakeeha AH, et al. 2024. Cs promoted Ni/ZrO_2-Al_2O_3 catalysts for dry reforming of methane: promotional effects of Cs for enhanced catalytic activity and stability. *Arabian Journal of Chemistry* 17:105564
[38] Al-Doghachi FAJ, Taufiq-Yap YH. 2018. CO_2 reforming of methane over Ni/MgO catalysts promoted with Zr and La oxides. *ChemistrySelect* 3:816–827
[39] Xu Y, Du XH, Li J, Wang P, Zhu J, et al. 2019. A comparison of Al_2O_3 and SiO_2 supported Ni-based catalysts in their performance for the dry reforming of methane. *Journal of Fuel Chemistry and Technology* 47:199–208
[40] Zhang X, Wang F, Song Z, Zhang S. 2020. Comparison of carbon deposition features between Ni/ZrO_2 and Ni/SBA-15 for the dry reforming of methane. *Reaction Kinetics, Mechanisms and Catalysis* 129:457–470